Validation of Simplified Load Equations Through Loads Measurement and Modeling of a Small Horizontal-Axis Wind Turbine Tower

Scott Dana, Rick Damiani, and Jeroen van Dam
National Renewable Energy Laboratory

NREL is a national laboratory of the U.S. Department of Energy
Office of Energy Efficiency & Renewable Energy
Operated by the Alliance for Sustainable Energy, LLC

This report is available at no cost from the National Renewable Energy Laboratory (NREL) at www.nrel.gov/publications.

Technical Report
NREL/ TP-5000-67562
April 2018

Contract No. DE-AC36-08GO28308

NREL
NATIONAL RENEWABLE ENERGY LABORATORY

Validation of Simplified Load Equations Through Loads Measurement and Modeling of a Small Horizontal-Axis Wind Turbine Tower

Scott Dana, Rick Damiani, and Jeroen van Dam
National Renewable Energy Laboratory

Suggested Citation
Dana, Scott, Rick Damiani, and Jeroen van Dam. 2018. Validation of Simplified Load Equations Through Loads Measurement and Modeling of a Small Horizontal-Axis Wind Turbine Tower. Golden, CO: National Renewable Energy Laboratory. NREL/TP-5000-67562.
https://www.nrel.gov/docs/fy18osti/67562.pdf

National Renewable Energy Laboratory
15013 Denver West Parkway
Golden, CO 80401
303-275-3000 • www.nrel.gov

Technical Report
NREL/ TP-5000-67562
April 2018

Contract No. DE-AC36-08GO28308

NOTICE

This report is available at no cost from the National Renewable Energy Laboratory (NREL) at www.nrel.gov/publications.

Available electronically at SciTech Connect http:/www.osti.gov/scitech

Available for a processing fee to U.S. Department of Energy and its contractors, in paper, from:

U.S. Department of Energy
Office of Scientific and Technical Information
P.O. Box 62
Oak Ridge, TN 37831-0062
OSTI http://www.osti.gov
Phone: 865.576.8401
Fax: 865.576.5728
Email: reports@osti.gov

Available for sale to the public, in paper, from:

U.S. Department of Commerce
National Technical Information Service
5301 Shawnee Road
Alexandria, VA 22312
NTIS http://www.ntis.gov
Phone: 800.553.6847 or 703.605.6000
Fax: 703.605.6900
Email: orders@ntis.gov

Cover Photos by Dennis Schroeder: (left to right) NREL 26173, NREL 18302, NREL 19758, NREL 29642, NREL 19795.

NREL prints on paper that contains recycled content.

Acknowledgments

The authors of this work would like to sincerely thank Paul Migliore of AnemErgonics, LLC, for allowing his tower and turbine to be used for the field measurement campaign of this study, without which this project would not have been realized.

Nomenclature

AWEA	American Wind Energy Association
C_d	coefficient of drag
DEL	damage equivalent load
DOFs	degrees of freedom
F_{blade}	rotor blade drag force
F_{nac}	nacelle drag force
F_{Tower}	tower drag force
F_{xshaft}	axial shaft load, as defined in International Electrotechnical Commission 61400-2
HAWT	horizontal-axis wind turbine
IEC	International Electrotechnical Commission
m	material slope from S/N curve, a.k.a., Wöhler exponent
M_{shaft}	combined bending moment for the shaft at the first bearing
M_{totalH}	tower-base moment caused by combined loads for Load Case H
M_{totalI}	tower-base moment caused by combined loads for Load Case I
M_{xb}	blade-root edgewise bending moment
M_{xshaft}	torque on the rotor shaft at the first bearing
M_{xt}	tower-base side-to-side bending moment
M_{yaw}	tower-base yaw moment (to complete tower-bending moment coordinate system)
M_{yb}	blade-root flapwise bending moment
M_{yt}	tower-base fore-aft bending moment
n	cycles in 20 years at rated rotor speed
NREL	National Renewable Energy Laboratory
NTM	normal turbulence model
NWTC	National Wind Technology Center
PSFs	partial safety factors
SLA	simplified loads approach
ST	shaft tilt
TS	tower shadow
ΔM_{tbn}	tower-base moment peak-to-peak load range as a result of axial shaft force

Table of Contents

List of Figures

List of Tables

1 Introduction

The International Electrotechnical Commission (IEC) 61400-2 provides three methods to derive design loads for small wind turbines (swept area <200 m^2). However, concerns have been raised about the validity of these methods. As part of a multifaceted effort to improve the modeling and prediction of small wind turbine dynamics, the National Renewable Energy Laboratory (NREL) tested a small, horizontal-axis wind turbine (HAWT) in the field at the National Wind Technology Center (NWTC). Researchers conducted a measurement campaign and parallel loads simulations to compare the three methods. Similar work was conducted in the past by [1], [2], and [3] on a small sample of turbines. There is still ample need to cover a range of turbine sizes, design features, and overspeed protection mechanisms to develop any strong conclusions. As a result, the information and data from this study can be used to tune safety factors and/or improve the design load derivation methods.

The test turbine was a 2.4-kilowatt (kW) downwind machine mounted on an 18-meter (m) multisection fiberglass composite tower. The tower of the system was instrumented and monitored for approximately 6 months. The collected data were analyzed to assess the turbine and tower loads and to further validate the simplified loads equations (or simplified loads approach [SLA]) from the IEC 61400-2 design standards. Field-measured loads were further corroborated using an aeroelastic model of the turbine. Ultimate loads at the tower base were assessed using both the simplified design equations (for parked conditions) and the aeroelastic model output (for operational cases). The simplified design equations in IEC 61400-2 do not comprehensively address fatigue loads. This project further compares the fatigue loads that were measured in the field to those predicted by the aeroelastic model and those calculated using the simplified design equations. For simplicity, no fault or idling situations were considered for this analysis. This report describes the collected data, analysis methods, aeroelastic modeling, and accompanying preliminary conclusions on the three methods prescribed by the IEC standards.

This paper is organized as follows. Section 2 summarizes the current status of IEC 61400-2 and the available methods for structural load determination. Section 3 introduces the test setup at the NWTC. Section 4 describes the aeroelastic modeling and the challenges that were encountered. Section 5 describes the simplified load approach results. Section 6 provides the preliminary results of the study.

2 Design Load Derivation Methods

The IEC 61400-2 "Wind turbines – Part 2: Small wind turbines" [4] standard comprises the design requirements for small wind turbines. One element of the requirements is the derivation of structural loads via any one of the following three methods:

1. Simplified loads approach
2. Aeroelastic modeling
3. Full-scale load measurements.

These methods are also referenced by the American Wind Energy Association (AWEA) small wind turbine standard [5].

The SLA, which can only be applied to certain turbine configurations (such as HAWTs with fixed hubs), includes a set of mathematical equations that readily provide design loads for the blades and main shaft, and from which other components' loads can be derived. Certain input parameters, such as design and maximum rpm and power, need to be based on measurements. This method was implemented at a time when aeroelastic simulations were time consuming and expensive, and thus provided an economical and quick solution to determine the design loads. As a result, the loads obtained using this method are generally conservative. Furthermore, the simplified design equations were developed to cover a wide of wind turbine designs and thus must capture the loads of the "worst-behaved" turbine within that population. Consequently, by using this method, there is less incentive to design a "better-behaved" turbine with a smaller load envelope. Finally, the SLA prevents the designer from fully appreciating the turbine system dynamics, because they are hidden behind the summary equations if not overlooked altogether.

Aeroelastic modeling uses flexible multibody dynamics software coupled with aerodynamic packages. The same software is also used for the design of utility-scale wind turbines (e.g., FAST, Bladed, FLEX, and so on). Small wind turbines often have additional degrees of freedom (DOFs) and other features that encumber accurate load prediction using simulation models, including free yaw, highly variable rpm, and passive aerodynamic controls (e.g., furling). Although mechanical load measurements for large turbines are mandated for model validation, only limited validation through measurements of power and rpm is required for small wind turbine models. Additionally, IEC 61400-1 [6] provides methods for the extrapolation of ultimate loads, but IEC 61400-2, although it requests extrapolation, does not include any methods for small wind turbines.

The third design load derivation method uses full-scale measurements following the approach described in IEC 61400-13 [7]. This method requires logging meteorological data and fundamental turbine loads (defined as blade-root moments, rotor moments, and tower-base moments). To obtain reliable loads, measurements must be taken over a wide range of external conditions (e.g., wind speed, turbulence, and so on) and operating conditions (e.g., normal power production, parked, startup and shutdown transients, and so on). It is worth noting that the latest revision of IEC 61400-13 will exclude load measurements for the purpose of design load derivation and limit the scope of the standard to validation of the aeroelastic model. In turn, the model is used to predict loads beyond the test conditions.

Within IEC 61400-2, each load derivation method has its own partial safety factors (PSFs) for loads in an attempt to cover the uncertainties related to the method (see Table 1).

Table 1. Partial Safety Factors for Loads from IEC 61400-2

Load Determination Method	Fatigue Loads	Ultimate Loads
Simplified loads approach	1.0	3.0
Aeroelastic modeling	1.0	1.35
Full-scale load measurements	1.0	3.0

To note, for fatigue damage calculations, IEC 61400-2 recommends a PSF of 10 for materials if a validated S-N curve is not used. This further denotes a large uncertainty with the currently allowed fatigue treatment.

After failures of a few small wind turbine systems in the United Kingdom that were certified to the IEC 61400-2 occurred, concerns have arisen about the validity of the SLA. Specifically, fatigue loads are thought to be underestimated by current practices. Experience by the Small Wind Certification Council (personal communication) showed that in some cases manufacturers rely on maximum thrust from IEC 61400-2 Load Case H to drive the tower-base design. Thus, fatigue loads from Load Case A may erroneously be believed to no longer be critical. Additionally, potential coupling between yawing and furling dynamics with tower vibrational modes is not captured by this process. Finally, designers may fail to apply the method in its entirety, instead rationalizing that the thrust loads from Load Case H or drag loads from Load Case I are overestimated. Consequently, designers then negotiate lower loads for that specific load case, not realizing that these load cases could be covering for a shortcoming in the fatigue load case. As a result, the IEC maintenance team for the IEC 61400-2 inserted warnings in the third edition of the IEC 61400.

Analogously, experience has shown that manufacturers tend to lower the PSFs across several load cases, or encourage using lower values for thrust and drag coefficients, thus reducing the level of conservatism in the SLA method while still applying the simplified equations.
It is clear that there is ample need for more data and investigation of the efficacy of the SLA, as well as of the capability of aeroelastic tools to capture important aspects of small wind turbine dynamics, including passive yaw behavior and coupling between turbine and tower modes. The shortcomings in the standards need to be better identified and quantified, which would allow for the development of more accurate load cases. In addition, the determination of structural loads could take advantage of a better representation of the turbine system dynamics, avoiding excessive conservatism.

3 Test Setup and Preliminary Results

As mentioned earlier, NREL tested a small horizontal-axis wind turbine in situ at the NWTC, with the intent of addressing the concerns indicated in Section 2, by comparing the three methods for load calculation. We anticipated that the testing would be conducted in two phases. The first phase targeted the tower loads, because they are relatively easy to measure and thus cost effective (no telemetry or slip rings needed); they are a good indication of the overall load level seen by the turbine; and, because the failures that occurred in the United Kingdom were attributed to tower fatigue failure. A second phase, which is not currently funded, would expand the load measurements to the blade roots and main shaft.

The turbine used in this study was chosen for two reasons: 1) The turbine was already installed at the NWTC, and 2) an existing FAST model was readily available. In addition, the turbine has important characteristics that are unique to small wind turbines, such as free yaw, variable speed, and stall control. Other characteristics include a rated power of 2.4 kW, downwind operation, and a rotor diameter of 3.7 m. The hub height was 18.18 m. Because this turbine operates downwind, it does not include a tail.

The composite free-standing tower was instrumented with strain gages at three different levels. The tower-base gages measured bending moments in two orthogonal directions and were located 863 mm above the tower-base hinge plate. Additional gages were placed 305 mm and 1,067 mm below the tower top (results for those gages are not reported in this study). The tower gages were calibrated by applying known loads to the tower top. The calibration process yields a cross-talk sensitivity matrix. This matrix is applied in postprocessing to determine tower loads relative to the tower coordinate system. For the tower loads reported in this report, a coordinate transformation was applied using the meteorological tower wind direction signal to resolve tower moments into the nacelle coordinate system. The wind direction was used rather than the nacelle-yaw position because the encoder sensor irreparably failed partially through the test campaign and was not repaired. Data from the encoder were used, however, to verify near-unity regression of turbine yaw angle with wind direction, as shown in Figure 1. The result of the coordinate transformation is a fore-aft bending moment denoted as $\boldsymbol{M_{yt}}$ and a side-to-side bending moment denoted as $\boldsymbol{M_{xt}}$. The yaw-moment $\boldsymbol{M_{yaw}}$ completes the right-hand coordinate system. Figure 2 illustrates the tower load components after applying the coordinate transformation.

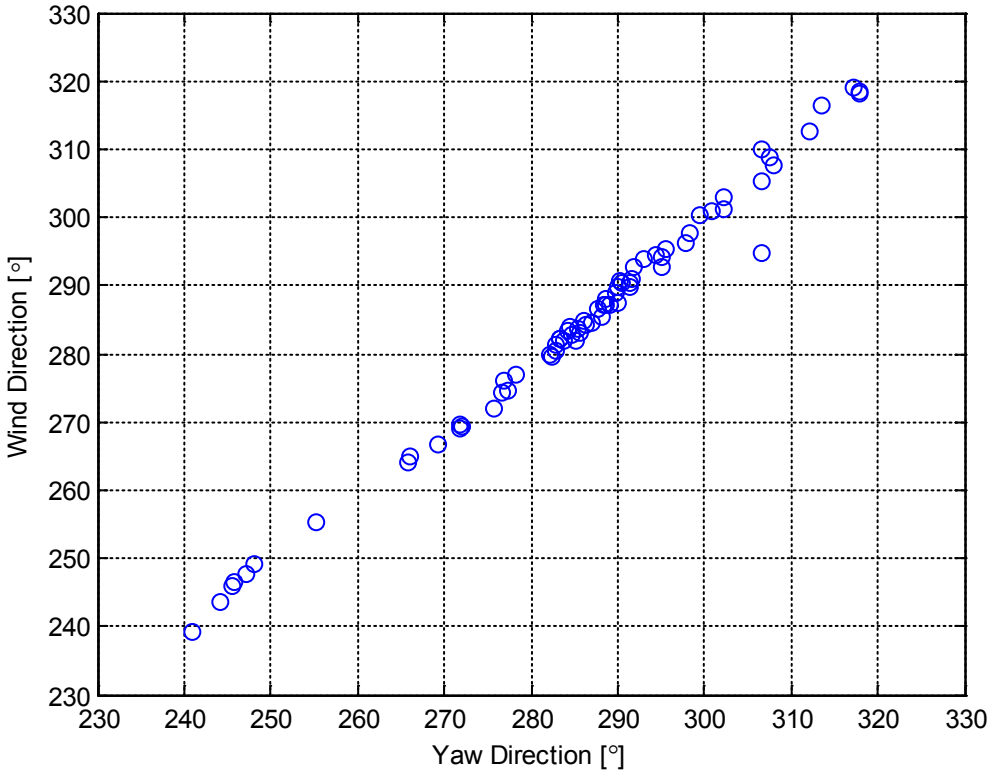

Figure 1. Wind direction correlation by measurement sector for wind speeds at rated (11 meters per second [m/s]) and above; 10-minute mean values plotted

A measurement sector was established in accordance with IEC 61400-12-1 to allow for accurate wind speed readings. As a result, all field-measured data were filtered to be within 223 to 333 degrees relative to true north.

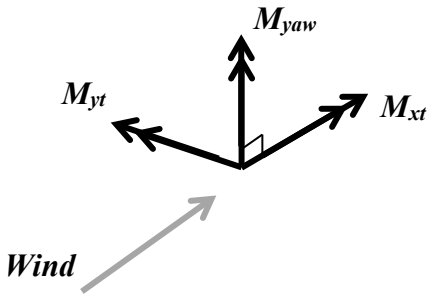

Figure 2. Tower loads operating moments by coordinate transformation

Data were recorded at 100 hertz (Hz) and stored in 10-minute long data files. Figure 3 shows the amount of captured data for normal operation by wind speed bin and turbulence-intensity level. The total number of 10-minute records for each wind speed bin is listed in Table 2. These data do not contain any fault conditions/events or idling. Startups and shutdowns were also acquired, with neither showing a significant impact on loads. Therefore, they were not reported.

For both extreme and fatigue loads, data were processed with postprocessing tools available at NREL (MExtremes and MLife). In particular, for fatigue calculations, a damage-equivalent load (DEL) was calculated for each channel of interest based on a Weibull distribution with a scale factor of 2 (i.e., Rayleigh distribution) of wind speeds over a 20-year design life and after binning load ranges of the rainflow-counted operating moments. Because this study focused on comparing results from different design approaches, no further accounting of load directionality as a function of wind direction (load roses) was done without loss of significance in the results. The assumed annual average wind speed for the IEC Class II machine used in this study is 8.5 m/s.

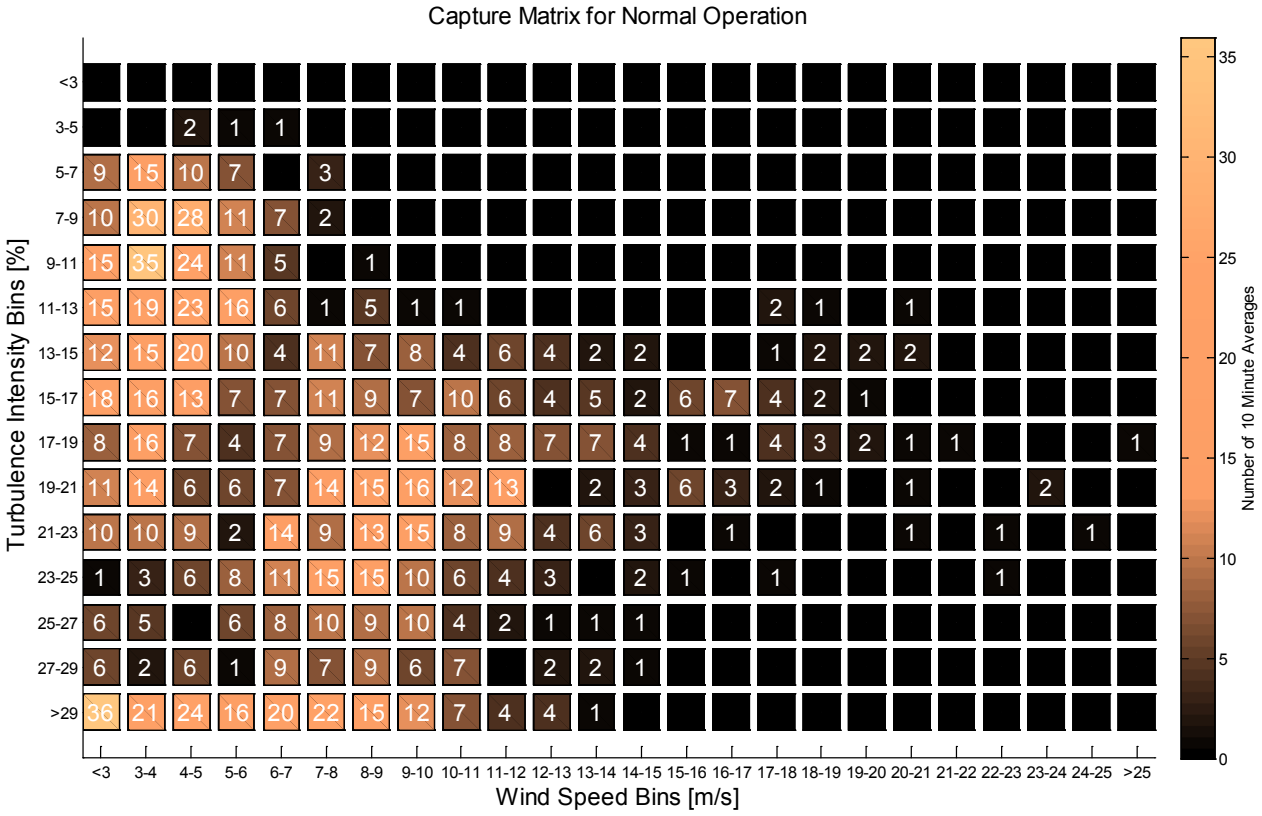

Figure 3. Capture matrix of all data collected within the valid measurement sector for normal turbine operation

Table 2. Number of 10-minute Data Files per Wind Speed Bin Within the Valid Measurement Sector

Wind Speed Bin (m/s)	Number of Files
<3	157
3–4	201
4–5	178
5–6	106
6–7	106
7–8	114
8–9	110
9–10	101
10–11	67
11–12	52
12–13	29
13–14	26
14–15	18
15–16	14
16–17	12
17–18	14
18–19	9
19–20	5
20–21	6
21–22	1
22–23	2
23–24	2
24–25	1
>25	1
Total Files	1,332

All data within the capture matrix for normal operation were postprocessed to 10-minute statistical values. The maximum, mean, and minimum fore-aft and side-to-side bending moments are presented in Section 6.

For fatigue calculations, all data collected during the measurement campaign were used. A summary of the wind speed distribution by bins is listed in Table 3. The third column represents the number of data files that have a mean wind speed within the corresponding bin range, and the fourth column lists the total elapsed time of the data files within each wind speed bin range. The

fraction of the turbine 20-year design life for each wind speed bin is listed in the last column. This distribution is based on the continuous Rayleigh distribution. Here, the distribution is discretized by selecting the fraction of life value found at each bin center of the wind speed bins from the continuous distribution. The fraction of life values, as a percentage, is plotted for each wind speed bin in Figure 4. The sum of these values is unity (100%).

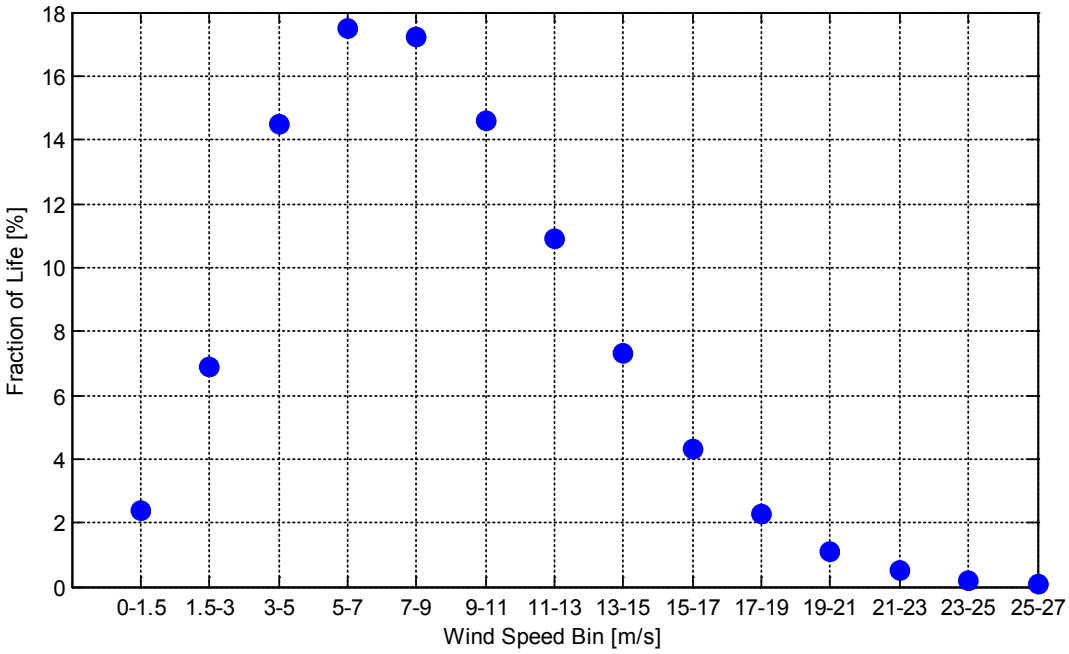

Figure 4. Fraction of life values and wind speed bin distribution based on a Rayleigh distribution for a 20-year design life

Table 3. Wind Speed Distribution of Data Files Used for Fatigue Calculations

Bin #	Bin Range	Number of Files	Elapsed Time of Power Production Files	Fraction of Life Spent in Bin
	(m/s)		(seconds [s])	
1	0.00 to 1.50	179	107,400	0.024
2	1.50 to 3.00	850	510,000	0.069
3	3.00 to 5.00	1,220	732,000	0.145
4	5.00 to 7.00	506	303,600	0.175
5	7.00 to 9.00	330	198,000	0.172
6	9.00 to 11.00	195	117,000	0.146
7	11.00 to 13.00	90	54,000	0.109
8	13.00 to 15.00	45	27,000	0.073
9	15.00 to 17.00	26	15,600	0.043
10	17.00 to 19.00	23	13,800	0.023
11	19.00 to 21.00	11	6,600	0.011
12	21.00 to 23.00	3	1,800	0.005
13	23.00 to 25.00	3	1,800	0.002
14	25.00 to 27.00	1	600	0.001

The lifetime, 1-Hz DELs for the tower-base operating moments were calculated using various Wöhler exponents with and without Goodman correction. However, for this study, only results without Goodman correction are presented. Three values for material slope ("**m**") were selected to cover the range of possible tower materials: 3, 6, and 10. An exponent of 3 is typical for steel towers, whereas an exponent of 10 is more common for fiberglass and other similar composites.

The DEL calculations were carried out using MLife, a MATLAB-based postprocessing tool developed by NREL to analyze wind turbine test data, and aeroelastic/dynamics simulations. MLife uses the one-pass cycle-counting method of Downing and Socie for fatigue cycle counting. For the analysis in this report, a cycle count of 0.5 was assigned to unclosed cycles. Other pertinent settings used for this fatigue analysis included 1,000 load-range bins, a Rayleigh distribution of wind speeds, and the design life was set at 20 years (630,720,000 seconds [s]). The resulting lifetime DEL values including cumulative fatigue spectra and short-term DELs are presented in Section 6.

4 Aeroelastic Modeling

The FAST model of the turbine and tower was provided by the manufacturer of the tower with approval from the turbine manufacturer. FAST is an aeroelastic simulation tool developed by the U.S. Department of Energy and NREL and is available publicly at no cost. For this study, FAST v 7.02 was used. FAST uses a combined modal and multibody representation of the tower, drivetrain, and blades to capture the structural dynamics of wind turbine systems (approximately 20 DOFs), and it is coupled to AeroDyn to capture blade aerodynamics as well as tail fin aerodynamics, while accounting for a prescribed torque (and pitch/yaw, generally speaking) control system algorithm.

The unsteady aerodynamics associated with a rapidly yawing rotor is quite complex, and it is not clear how well the tool performs for certain configurations (e.g., with passive-yawing, downwind rotors).

For the modeling discussed in this paper, normal turbulence model (NTM) wind files were created at reference wind speeds (U_{ref}) of 2, 4,…,24, 26 m/s. A turbulence characteristic of 18% was used per guidance in [4]. To generate time-series realizations of turbulence, three random seeds were selected for each reference wind speed. Air density was set to test site conditions of 1.0 kg/m^3.

FAST v 7.02 does not account for loads coming from tower aerodynamic drag. We tried to assess its importance from a tower-base loading perspective. For example, the tower-base bending moment caused by the reported maximum thrust of the turbine is approximately 50 kilonewton meters (kNm) at 18 m/s for the turbine and tower configuration described in this paper. Using the same wind speed and coefficient of drag (C_d) values of 0.7 (typical for cylinders) and 1.096 (provided by tower designer), tower drag yields approximate base moment values of 4.7 kNm and 7.3 kNm. The ratio of this tower drag moment to maximum rotor thrust moment thus amounts to 9.4% and 14.6%. Although the importance of the tower-base moment may be minimal under operational conditions, tower drag may still affect dynamics aspects as it virtually increases damping of the system and contributes to tower loading under parked (extreme winds) conditions.

The aeroelastic simulations produced evidence of the turbine not tracking the wind directional changes, which was also observed in the field (recall Figure 1). Moreover, the baseline model results (with NTM) revealed a consistent yaw bias that grew with increasing wind speeds. Figure 5 illustrates the observed yaw bias artifact for an NTM wind file with a reference wind speed of 20 m/s. We initially believed that the yaw bias may be caused by wrong estimates of the tower-top inertial and damping properties that affect modal coupling between turbine yawing and tower bending. As a result, we investigated the FAST model to identify the source of yaw bias and better understand the reasons for seemingly overactive yaw dynamics. The details of this investigation are provided in Appendix A.

In spite of these model shortcomings, the resulting loads obtained using the NTM wind files were included in this study. The model data were analyzed in the same manner as the field-measured data. Both extreme loads and fatigue DELs were obtained, and the comparisons with field data are given in Section 6.

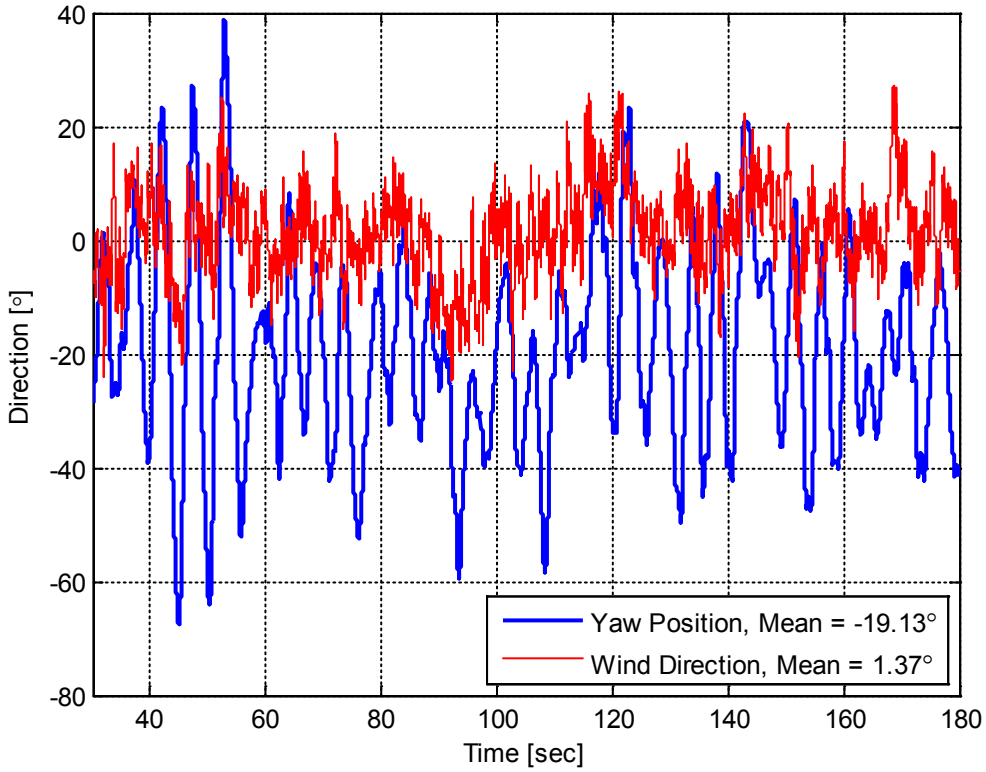

Figure 5. FAST model output illustrating the presence of a yaw bias and large magnitude yaw oscillations

5 Simplified Loads Approach

For the SLA, the input parameters were derived from the FAST model input deck, preliminary test results, and some measurements taken of the test turbine. Only Load Cases H and I were found relevant for tower-base ultimate loads. Load Case A is the only SLA fatigue case. A summary of the loads for each of these load cases are found in Table 4, Table 5, and Table 6. For consistency between all loads analysis approaches, air density was set to test site conditions of 1.0 kg/m^3.

Table 4. SLA Load Case A Loads Summary

Load Component	M_{xb} Newton meters (Nm)	M_{yb} (Nm)	M_{xshaft} (Nm)	F_{xshaft} (N)	M_{shaft} (Nm)
Load Case A*: normal operation	77	118	68	286	147

*Loads are ranges

Table 5. SLA Load Case H Loads Summary

Load Component	M_{yb} (Nm)	F_{xshaft} (N)	F_{nac} (N)	F_{tower} (N)
Load Case H: extreme wind	559	1,803	344	4,647

Table 6. SLA Load Case I Loads Summary

Load Component	F_{Tower} (N)	F_{blade} (N)	F_{nac} (N)
Load Case I: parked wind loading, max exposure**	2,370	420	175

** Maximum exposure of the turbine is aligned with the wind

The SLA only specifies loads for the blade root, turbine shaft, and tower top. These loads thus have to be extrapolated to the tower base for comparison with the test data and aeroelastic model. All design load cases were calculated in this analysis; however, for this turbine and tower configuration, the design drivers for the tower base are Load Cases H and I. For Load Case H and I, the drag loads on the rotor, nacelle, and tower are included when determining the tower-base bending moment.

Load Case A is used for fatigue load estimates. Here, the peak-to-peak axial shaft load, ΔF_{xshaft}, was used to calculate the fore-aft tower-base bending moment, and the rated rotor speed was used to derive the number of cycles in the 20-year design life. These fatigue failure calculation parameters are listed in Table 7, where ΔM_{tbn} is the tower-base moment peak-to-peak load range for fatigue assessment and n is the number of fatigue cycles in the 20-year design life.

Table 7. SLA Fatigue Failure Calculation Parameters

Parameter	Value
ΔM_{tbn} (Nm)	5183
n [cycles]	1.04E10

6 Comparison of Methods

6.1 Ultimate Loads

For ultimate loads, the comparison of the three methods is most problematic, because field measurements cannot readily render loads under the same load cases analyzed under either SLA or aeroelastic modeling. Thus, extrapolation of the measured loads would be needed; this has not been completed at this time.

The latest revision of IEC 61400-1 provides three methods for load extrapolation for DLC 1.1 (power production case) that require different additional load factors. These load factors are listed in Table 8. IEC 61400-2 does not explicitly mention the need for load extrapolation of aeroelastic simulations. This difference between large and small wind turbine design approaches may not be fully justified. This aspect was not investigated in this study, but we plan on including it in upcoming research.

Table 8. Load Factors Associated with Extrapolated Peak Loads (from IEC 61400-1 Latest Edition)

Method	Additional Load Factor
Mean of extremes	1.35
Extrapolation to 99%	1.2
Extrapolation to 50 year	1.0

For this paper, neither load extrapolation nor a load factor was applied. Figure 6 and Figure 7 illustrate the comparison of ultimate loads between all three methods for the fore-aft and side-to-side directions, respectively. Overall, there is good agreement between the field-measured bending moments and the FAST predictions, particularly for the side-to-side values. However, for wind speeds at and above 18 m/s, the FAST maxima begin to deviate appreciably from the field-measured maxima in the fore-aft direction. Consequently, the mean values do not trend at these wind speeds. In general, the FAST maxima exhibit an upper-bound trend of the field maxima values. This discrepancy may be caused in part to an oversimplified control system used in the FAST model, wherein a single speed versus a torque curve is used for control. The actual turbine control scheme is more complex.

The maximum tower-base bending moments for Load Case H and I are listed in Table 9. For Load Case H and I, each component moment contribution is listed along with the total moment for the respective load case. The red dashed lines in Figure 6 and Figure 7 represent the SLA load envelope for Load Case I. Load Case I assumes a reference wind speed of 42.5 m/s and a parked condition of the turbine. Meaning, this load case cannot be directly compared to the field loads and FAST predictions; however, the load envelope line illustrates that the FAST predictions and field loads are within this envelope for the captured wind speeds. A load envelope line for Load Case H, which assumes a wind speed of 59.5 m/s, was not inserted in these figures because of the large magnitude of this bending moment in comparison to the maximum moment from Load Case I. Similar to Load Case I, Load Case H cannot be directly compared to the field loads and FAST predictions. Extrapolation of the field-measured loads out to the design wind speeds of Load Case H and I are required for a direct comparison.

Table 9. Load Case H and I Bending Moment Results at the Tower Base

Load Case	Component Contributions to Total Bending Moment			Total Moment (Nm)
	Rotor Drag (Nm)	Nacelle Drag (Nm)	Tower Drag (Nm)	
H	32,625	6,222	41,355	80,202
I	21,099	22,781	3,174	47,055

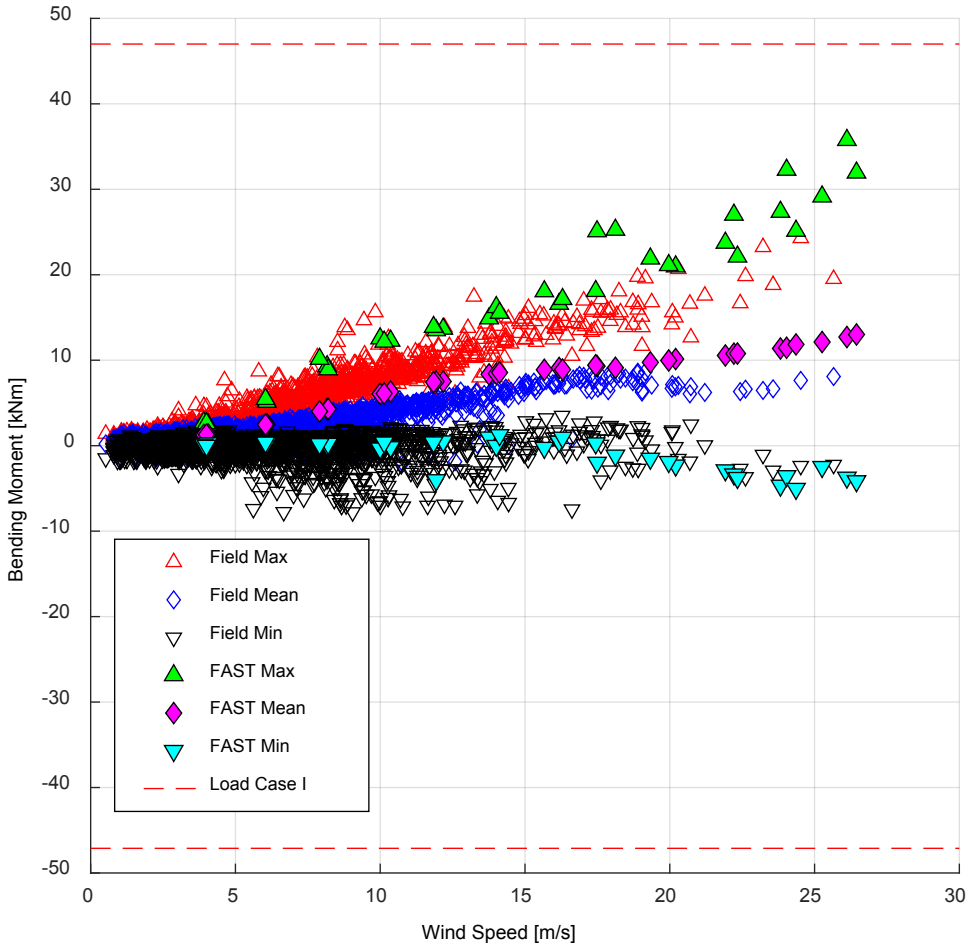

Figure 6. Ten-minute statistical comparison of field and FAST fore-aft tower-base loads with an SLA load envelope

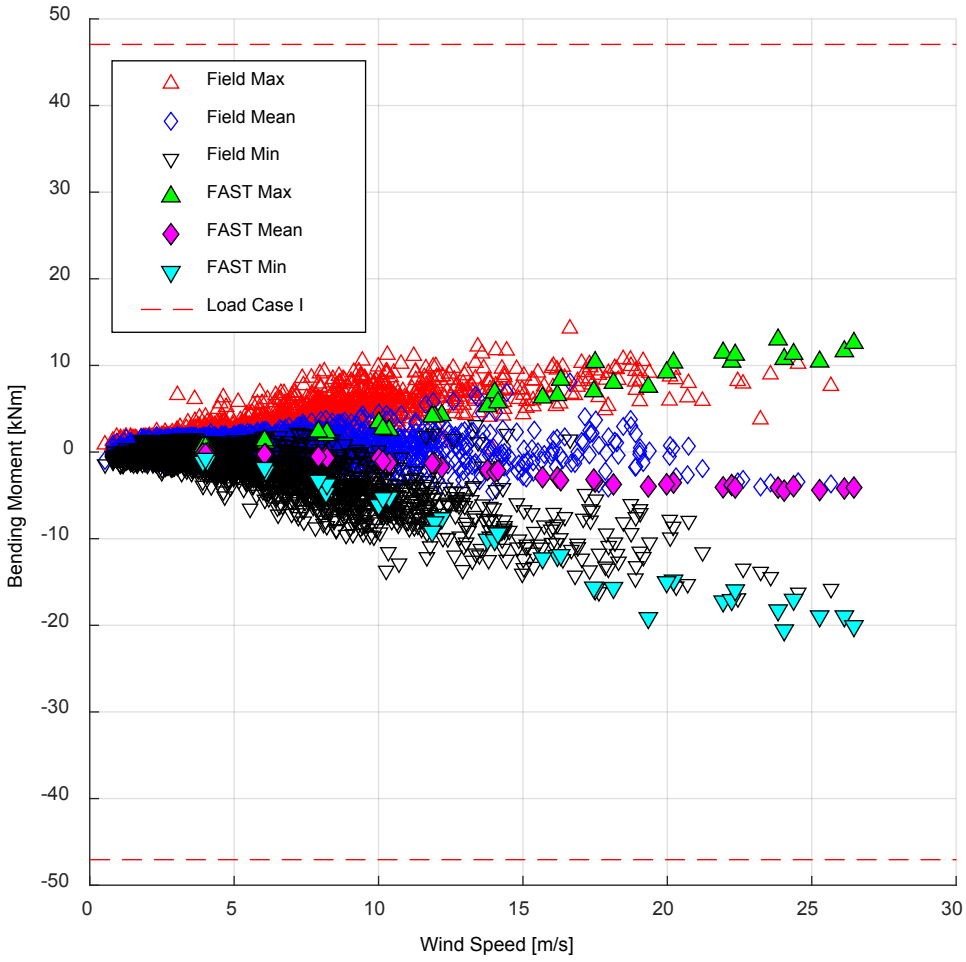

Figure 7. Ten-minute statistical comparison of field and FAST side-to-side tower-base loads with an SLA load envelope

6.2 Fatigue Loads

The SLA only considers fatigue loads from normal operation (i.e., Load Case A). A constant amplitude range with a large number of cycles (assuming the turbine runs at nominal rotor speed for the entire design life) is calculated. The amplitude range and fatigue cycles from Table 7 were used to determine DELs for the same three S-N curve values: 3, 6, and 10. For direct comparison, all DELs were scaled to a reference cycle value that is equivalent to 1 Hz for 20 years ($6.3*10^8$ cycles). The 20-year lifetime 1-Hz DELs for the field and FAST loads are presented in Table 10 along with the SLA DELs. Table 10 presents the DELs at zero mean without Goodman correction.

Table 10. Tower-Base Lifetime DELs at Zero Mean Without Goodman Correction for Various S-N Curves

		Field DELs		FAST DELs		SLA DELs
		Fore Aft (kNm)	Side to Side (kNm)	Fore Aft (kNm)	Side to Side (kNm)	Fore Aft Only (kNm)
m	**3**	2.7618E+000	2.0940E+000	3.8038E+000	3.3075E+000	1.3195E+001
	6	5.4034E+000	4.4606E+000	7.1352E+000	7.0167E+000	8.2701E+000
	10	8.5963E+000	7.7233E+000	1.1496E+001	1.0908E+001	6.8603E+000

Table 10 shows that the method resulting in the maximum fatigue loading is highly dependent on the slope of the S-N curve. This is because of how the DEL is calculated, and how high load ranges with lower occurrence versus low load ranges with higher occurrence can be transferred to the reference cycles, N_{eq} (see Figure 8). The figure illustrates how the DEL calculated for the load range and cycles (S_1, N_1) for an S-N slope of 10 ($S_{1eq,m=10}$) is greater than the corresponding DEL for (S_2 , N_2) ($S_{2eq,m=10}$). The reverse is true when comparing $S_{1eq,m=3}$ and $S_{2eq,m=3}$. Note that the SLA produces a spectrum consisting of a small load range with a large number of cycles when compared to aeroelastic modeling and field-derived data. Figure 9 also shows the difference in distributions between FAST and the measured loads.

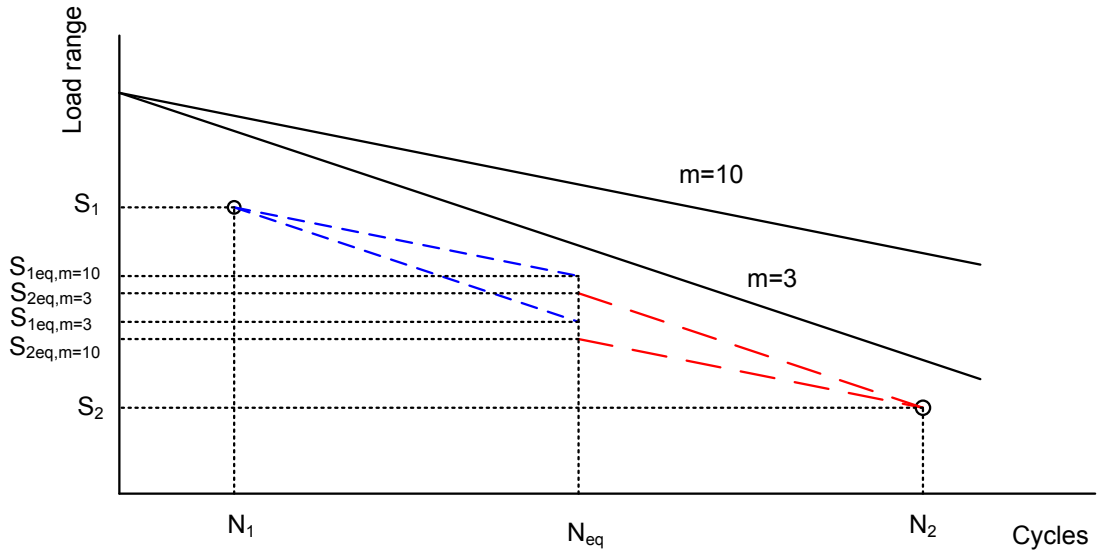

Figure 8. Illustration of the effect of the chosen S-N curve slope on the DEL for the high-load range at a low number of cycles and vice versa

In Figure 9, the rainflow-cycles have been cumulatively summed within each load-range bin. Overall, the FAST fatigue spectra had a steeper slope with more cycles at high load ranges and fewer spectra at low loads ranges when compared to the field spectra. This outcome can be attributed to the overprediction of high-range loads by FAST, as observed in the ultimate loads comparison.

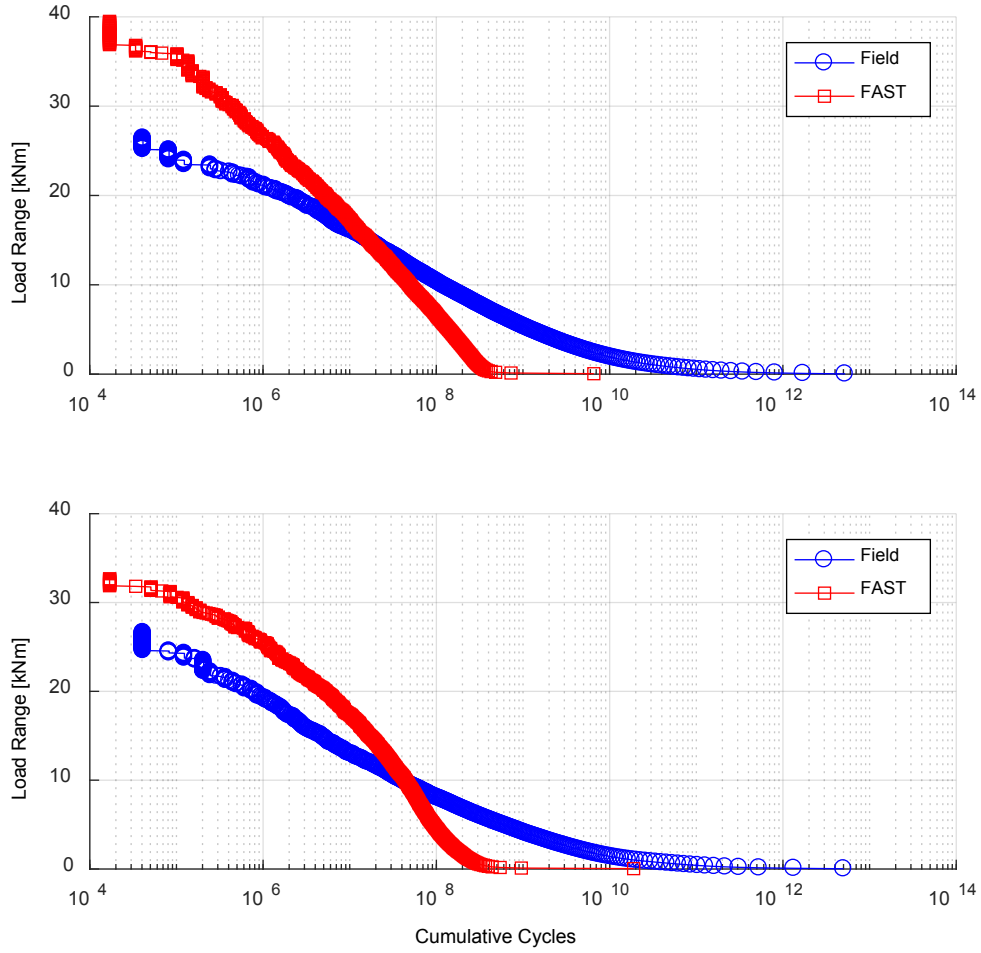

Figure 9. Fore-aft (top) and side-to-side (bottom) moment cumulative fatigue spectra comparison for field-measured loads and aeroelastic output

A final fatigue comparison is presented in Figure 10. Here, a short-term DEL has been calculated for each 10-minute data file. The DELs have been plotted versus the corresponding mean wind speed of each 10-minute data file. The side-to-side DELs (Figure 10 [bottom]) show good agreement between the field and FAST loads, as was the case for the ultimate loads comparison. The fore-aft DELs deviate more consistently with the ultimate loads comparison.

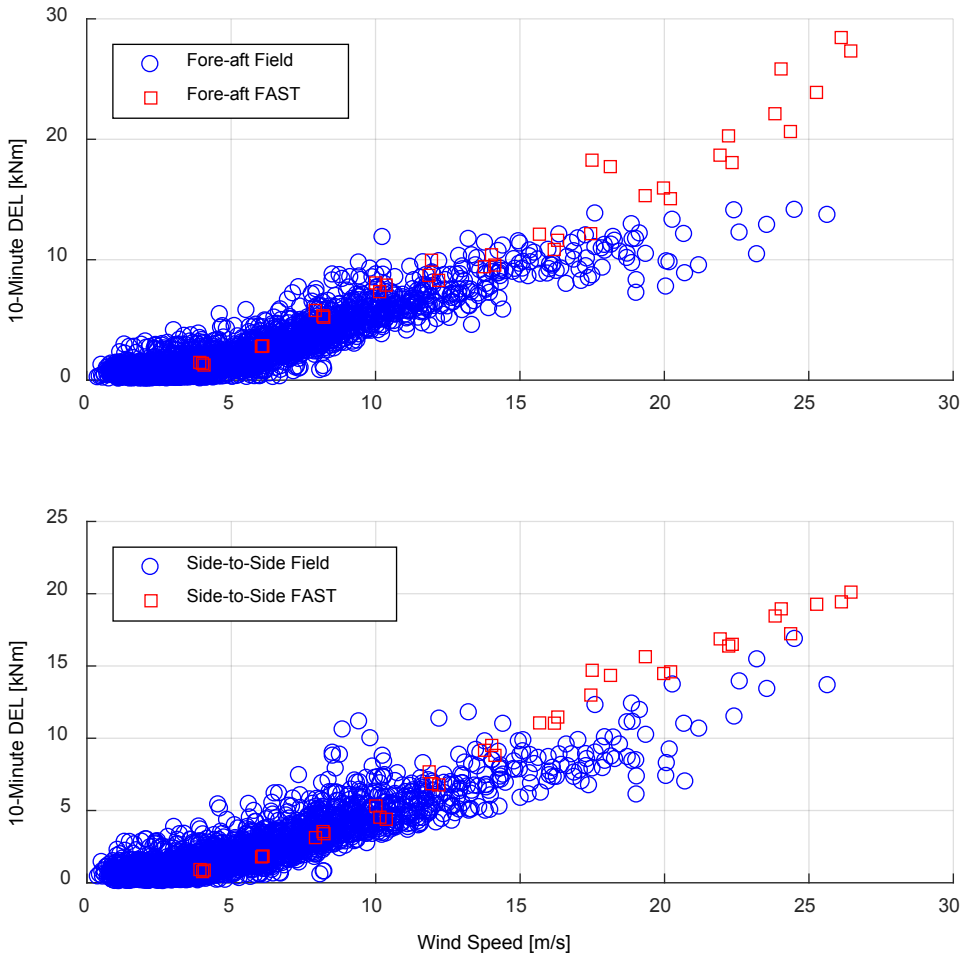

Figure 10. Short-term (10-minute) fore-aft (top) and side-to-side (bottom) DELs without Goodman correction versus mean wind speed for a material slope of 10

7 Conclusions and Future Work

The three available methods for deriving design loads were applied to a small wind turbine to generate data to allow for the comparison and refinement of the methods. In this study, the focus was on the tower-base bending moments to provide an indication of the overall performance of the methods.

The FAST model output showed a consistent yaw error under operational load case simulations, which cannot be easily explained. Several parameters were evaluated for their impact on the observed yaw error. We observed that the tower-top deflection had an important role on the yaw bias. Additionally, when compared to the field measurements, the simulations showed an overall yaw behavior that was more active. This outcome may be caused by a coupling between turbine yaw and tower dynamics also driven by a less-than-perfect representation of the tower modal properties. It is expected that by adding tower aerodynamic drag to the model (not available in the version of FAST used in this study), the resulting additional damping may reduce this yaw motion.

Despite the discrepancy in observed yaw dynamics, there is good agreement on tower loads between those measured in the field and those predicted by the FAST simulations under normal power production, at least for wind speeds up to 18 m/s. Above this wind speed, the FAST-derived loads exceed the measured loads. Because of the observed yaw error and the absence of tower drag in FAST, this difference can only be explained by an incorrect modeling of either the controller behavior, the tower dynamics, or both. To allow a proper comparison of FAST outputs to the field measurements and the SLA-derived data, measurements under a high wind speed with the turbine parked would need to be analyzed and extrapolated. Additionally, the design load cases for extreme winds would need to be run with FAST and analyzed. This analysis is part of proposed future work.

The fatigue spectra for the measured and simulated tower-base moments look quite different with FAST having more large-amplitude load ranges and fewer small-amplitude load ranges. The overall 20-yr, 1-Hz DELs for all methods show significant differences and are highly dependent on the assumed slope of the tower material. It should be noted that these fatigue values can be directly compared because the PSF for loads for all three methods is 1.0.

In general, the following observations are made:

- For free-yaw turbines, data may be needed to properly tune the aeroelastic model.
- Only limited data are available to validate proper modeling of downwind turbines in FAST.
- For small wind turbines, tower drag can have a significant contribution to tower-base loads at high wind speeds and, as such, it is recommended that they be included in the aeroelastic model. For future work, we plan to compare measured loads under high wind speeds in which the turbine is parked.

Additional future work will include the verification of a tower section against the three methods, the inclusion of mean loads for fatigue load assessments, and a better evaluation of tower drag loads. Further research will need to address the tower damping coefficient used in the model and

how that impacts the calculated loads. Developing an affordable method for determining the damping values or establishing good default values should also be considered.

References

1. Van Hulle, F. J. L., P. P. Soullié, H. Seifert, Ch. Hinsch, P. Zorlos, A. Derrick, P. Højholdt. 1996. *Verification of Design Loads for Small Wind Turbines*, Final Report Joule Project CT93-0423, ECN-C--96-033. ftp://ftp.ecn.nl/pub/www/library/report/1996/c96033.pdf.

2. Jonkman, J., J. van Dam, T. Forsyth, D. Davis. 2003. "Investigation of the IEC Safety Standard for Small Wind Turbine Design Through Modeling and Testing." Presented at the 41st AIAA Aerospace Sciences Meeting and Exhibit, January 6–9, 2003, Reno, Nevada, pp. 340-350. https://www.nrel.gov/docs/fy03osti/33004.pdf.

3. Prascher, D. and A. Huskey. 2004. "Tower Design Load Verification on a 1-kW Wind Turbine." NREL/CP-500-37112. National Renewable Energy Laboratory (NREL), Golden, CO (US). https://www.nrel.gov/docs/fy05osti/37112.pdf.

4. International Electrotechnical Commission (IEC). 61400-2 ed 3.0 Wind turbines – Part 2: Small wind turbines, 2013-12.

5. American Wind Energy Association. AWEA Small Wind Turbine Performance and Safety Standard, AWEA Standard 9.1 (2009).

6. IEC 61400-1 ed 3.1 Wind turbines – Part 1: Design requirements, 2014-04.

7. IEC 61400-13 Wind turbine generator systems – Part 13: Measurement of mechanical loads, 2001-06.

Appendix A

Investigation of Observed Yaw Bias in the FAST Model Output

During this study, potential contributing variables to a yaw bias were first removed or modified and then reintroduced to quantify their effects. The following parameters were investigated:

- Turbulence
- Rotor imbalance (pitch and mass)
- Shaft tilt
- Tower shadow
- Tower degrees of freedom (DOFs).

To exclude the possibility of code changes between the currently used FAST v7.02 and the previous version v6.01 (original to the received model input files), the model input deck was also run with FAST v6.01. No differences were noted in the yaw bias trend.

Turbulence

To reduce or eliminate yaw oscillations and, consequently, preserve any yaw bias, the normal turbulence model wind files were replaced by steady wind speed (no shear and no turbulence) and wind direction files. Reference wind speeds of 12, 16, and 20 meters per second (m/s) and a fixed wind direction of zero degrees were used. The resulting yaw errors for these cases are presented in Figure A1. After a transient of approximately 20 seconds (s), a yaw bias remained for all wind speeds. Notably, the yaw error decreased with increasing wind speed. This outcome is the opposite trend observed using the normal turbulence model wind files. Further, these results suggest that turbulence does not have a significant contribution to yaw bias as expected.

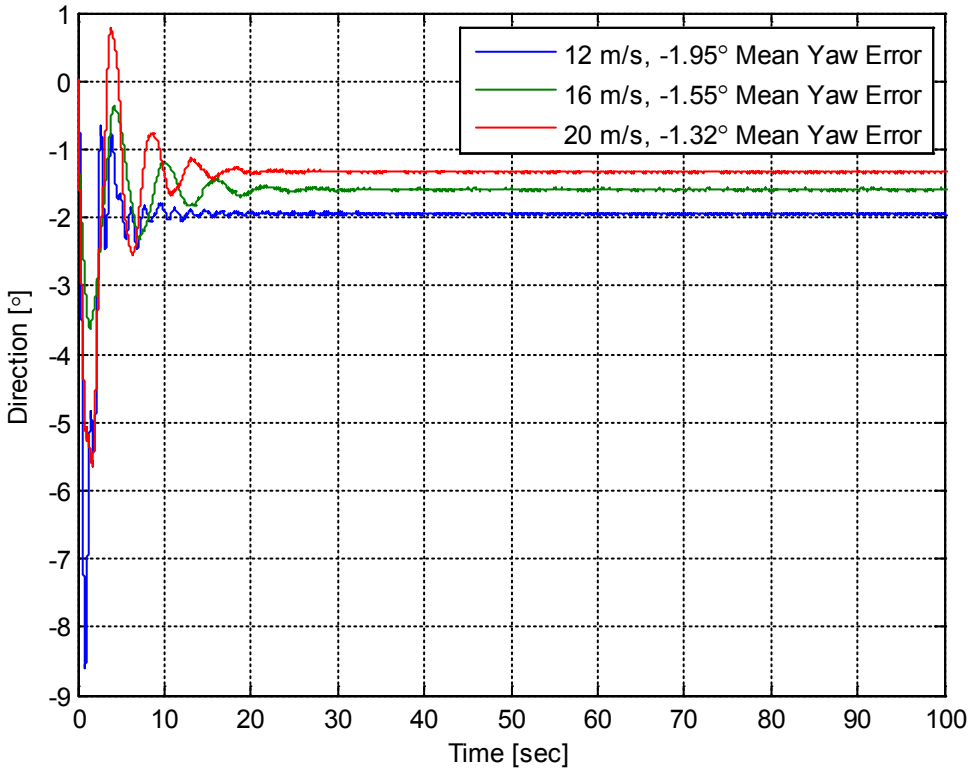

Figure 11. Yaw errors at 12 m/s, 16 m/s, and 20 m/s steady-state wind speed and direction

Rotor Imbalance

The baseline model contained slight pitch and mass imbalances in accordance with aeroelastic modeling guidelines. To ensure these asymmetries were not contributing to the yaw bias, we removed them. The model output revealed no change in yaw bias as reported in Figure A1 for all three steady-state wind speeds.

Shaft Tilt

The baseline model had a shaft tilt of 3 degrees. Shaft tilt was set to 0 degrees and the model was run for all three steady wind speeds. The resulting steady-state yaw error output is presented in Figure A2. The yaw errors increase compared to the baseline model, but a trend with wind speed is not clear for the three wind speed metrics used here. Overall, this modification has a negative impact on the yaw bias.

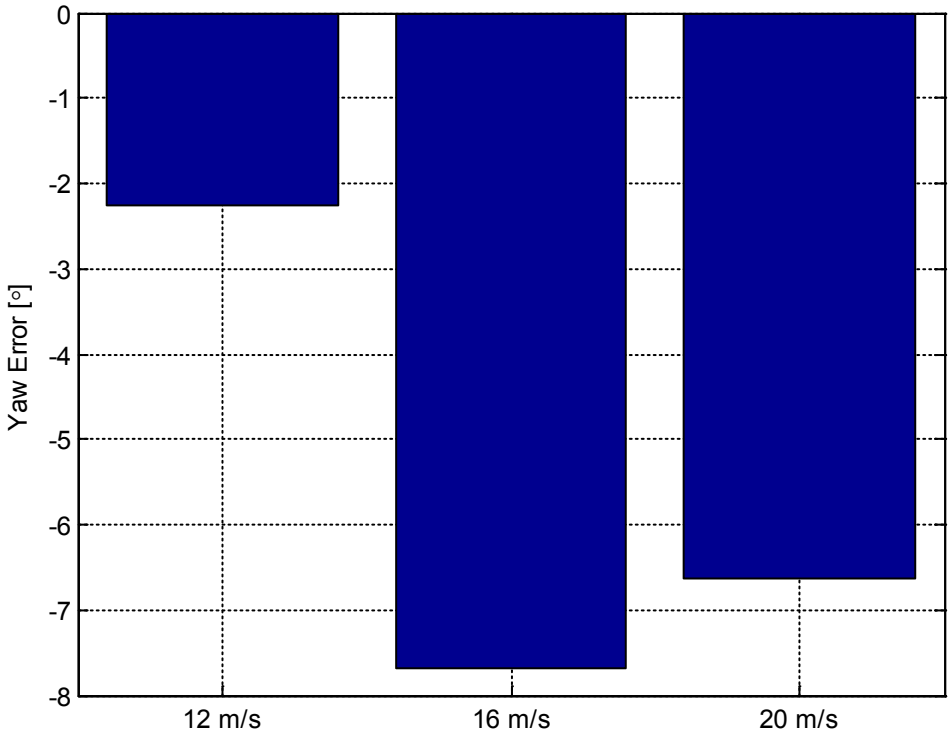

Figure 12. Yaw error for steady state wind speeds and direction with the shaft tilt set to 0 degrees

Yaw Moment Study

Next, the yaw moment was investigated as a function of yaw angle to assess any potential equilibrium point away from 0-degree yaw. The yaw DOF was disabled in the model and the yaw position was fixed at various angles above and below 0 degrees. For simplicity, only yaw moments using the 16 m/s steady-state wind file were used. Figure A3 shows the final result of this approach in which the maximum, mean, and minimum yaw moment values are plotted for each yaw angle. The spread in yaw moment generally grows with yaw error. The curve's constant slope around 0 degrees indicates that there is a restoring moment for small yaw angles. Yaw stable equilibrium is found at approximately 1 degree, where the mean yaw moment changes sign.

This process was repeated with all sources of asymmetry removed, i.e. no rotor imbalance, all pitch angles set to zero degrees, tower shadow set to zero, and shaft tilt set to 0 degrees. The same yaw moment trend remained, although the yaw moment spread between the maxima and minima values was slightly reduced.

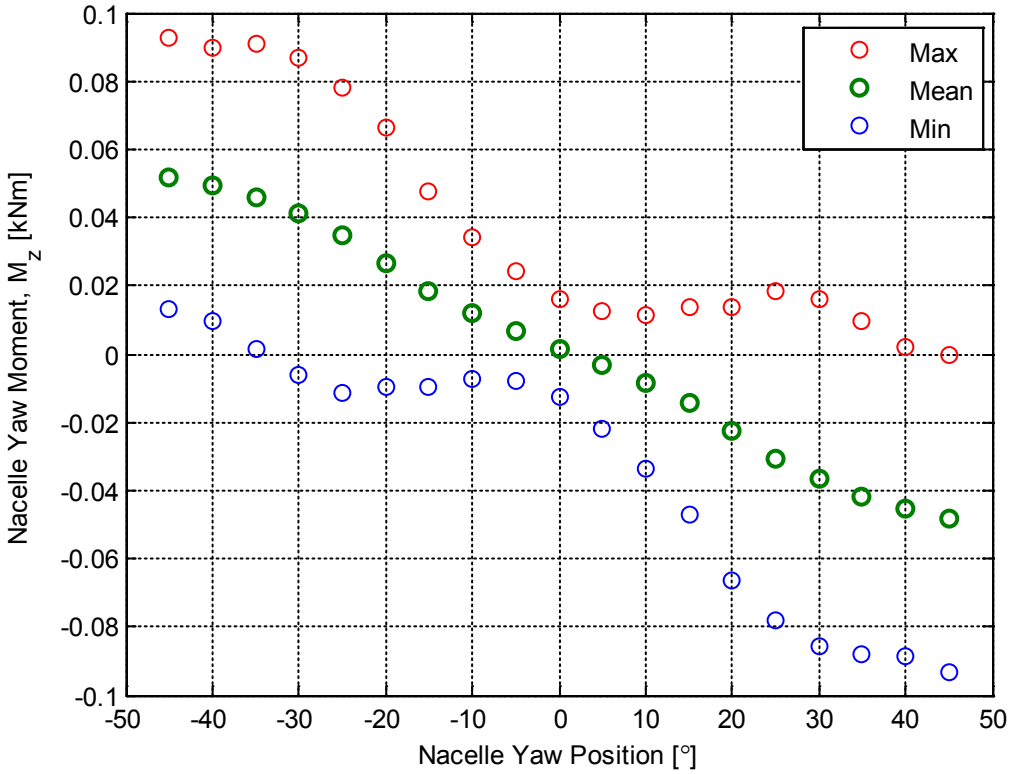

Figure 13. Yaw moment as a function of fixed yaw angle at the 16-m/s steady wind speed

Tower Flexibility and Tower Shadow Effects

Next, we removed the tower DOFs to exclude tower flexibility from the yaw bias issue. Figure A4 shows the yaw error resulting from this study. Again, only the steady-state response of the simulation was used. In contrast to Figure A1, wherein tower DOFs were enabled, the yaw error is now positive and increases significantly for the 16-m/s and 20-m/s cases. The yaw error magnitudes showed better agreement with those in Figure A2, when the shaft tilt was set to 0 degrees.

To further explore the model sensitivity to shaft tilt and tower DOFs, we ran additional simulations with various shaft tilt values. Tower shadow was also varied to quantify this parameter's effect. For simplicity, only the 16-m/s steady wind file was used. Tower DOFs remained disabled while tower shadow and shaft tilt values were adjusted. Figure A5 illustrates the results of these runs. In the x-axis labels, TS refers to tower shadow ("on" or "off") and ST refers to shaft tilt (0 or 3 degrees). The largest yaw errors exist when the shaft tilt is at the baseline model setting of 3 degrees. Yaw errors are at a minimum when the shaft tilt is 0 degrees. Additionally, the tower shadow has been shown to have a small effect on yaw bias.

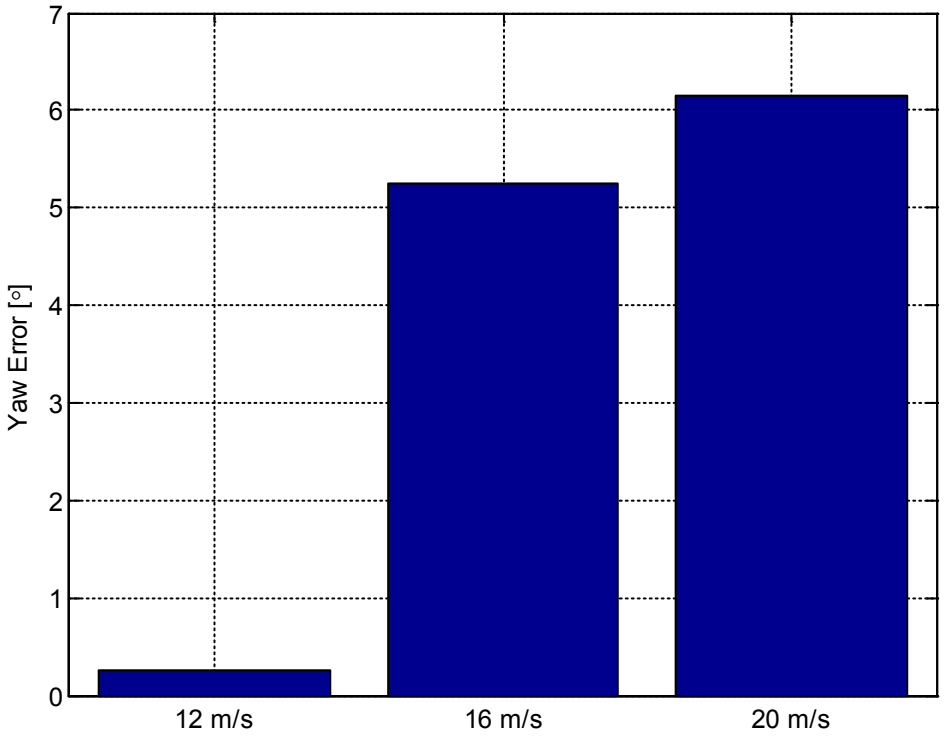

Figure 14. Yaw error using the baseline model setting with tower DOFs disabled

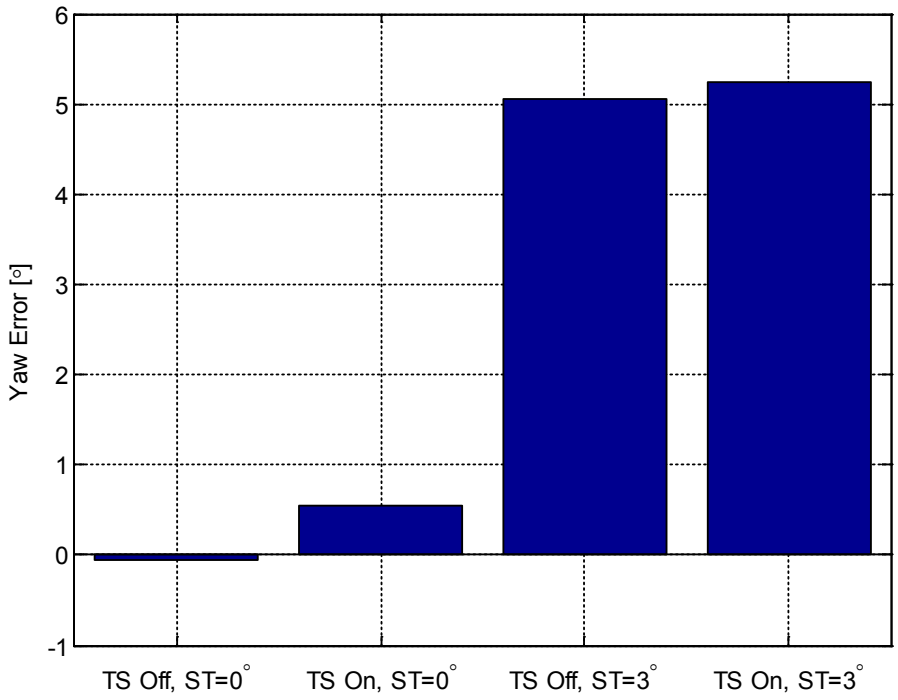

Figure 15. Yaw error at 16-m/s steady wind with tower DOFs disabled and varied tower shadow (TS) and shaft tilt (ST) values

Comparing Figure A1 and Figure A5 reveals that the shaft tilt can be negated by the flexibility of the tower. This outcome is similarly represented in Figure A5, when the tower is not free to

deflect. Here, a shaft tilt value of zero reduces the yaw bias. Conversely, when the tower is not free to deflect (tower DOFs disabled) and shaft tilt is 3 degrees, the yaw bias reaches a maximum, because of the shaft torque contribution about the vertical axis.

Final Observations on Yaw Error Trends and Model Output Data

Shaft tilt and tower flexibility were observed to have the largest contributions to yaw bias but there are other model inputs that may contribute. The tower mode shape coefficients included with the baseline tower model are not unique for side-to-side and fore-aft modes. However, in reality, a slight difference between these coefficients would be expected. This inaccuracy may be influencing the yaw dynamics. The yaw damping coefficient is not known with absolute certainty. An increase in yaw damping will help attenuate the large yaw oscillations and possibly lead to better yaw tracking; however, tuning this parameter will not remove the yaw bias.